SLAC-PUB-5402
DESY 91-089
December 1990
(E)

Measurement of the Decay of the $\Upsilon(1S)$ and $\Upsilon(2S)$ Resonances to Muon Pairs

The Crystal Ball Collaboration

M. Kobel[6], D. Antreasyan[9], H.W. Bartels[5], D. Besset[11], Ch. Bieler[8], J.K. Bienlein[5], A. Bizzeti[7], E.D. Bloom[12], I. Brock[3], K. Brockmüller[5], R. Cabenda[11], A. Cartacci[7], M. Cavalli-Sforza[2], R. Clare[12], A. Compagnucci[7], G. Conforto[7], S. Cooper[a,12], R. Cowan[11], D. Coyne[11,2], A. Engler[3], K. Fairfield[12], G. Folger[6], A. Fridman[b,12], J. Gaiser[12], D. Gelphman[12], G. Glaser[6], G. Godfrey[12], K. Graaf[8], F.H. Heimlich[8,7], F.H. Heinsius[8], R. Hofstadter[12], J. Irion[9], Z. Jakubowski[4,5], H. Janssen[10], K. Karch[5], S. Keh[13], T. Kiel[8], H. Kilian[13], I. Kirkbride[12], T. Kloiber[5], W. Koch[5], A.C. König[10], K. Königsmann[c,13], R.W. Kraemer[3], S. Krüger[8], G. Landi[7], R. Lee[12], S. Leffler[12], R. Lekebusch[8], T. Lesiak[4], A.M. Litke[12], W. Lockman[12], S. Lowe[12], B. Lurz[6], D. Marlow[3], H. Marsiske[5,12], W. Maschmann[8,5], P. McBride[9], F. Messing[3], W.J. Metzger[10], H. Meyer[5], B. Monteleoni[7], B. Muryn[d,4], R. Nernst[8], B. Niczyporuk[12], G. Nowak[4], C. Peck[1], P.G. Pelfer[7], B. Pollock[12], F.C. Porter[1], D. Prindle[3], P. Ratoff[1], M. Reidenbach[10,5], B. Renger[3], C. Rippich[3], M. Scheer[13], P. Schmitt[13,9], J. Schotanus[10], J. Schütte[6,9], A. Schwarz[8,12], D. Sievers[8], T. Skwarnicki[5], V. Stock[8], K. Strauch[9], U. Strohbusch[8], J. Tompkins[12], H.J. Trost[5], B. van Uitert[12], R.T. Van de Walle[10], H. Vogel[3], A. Voigt[5], U. Volland[6], K. Wachs[5], K. Wacker[12], W. Walk[10], H. Wegener[6], D. A. Williams[9,2], P. Zschorsch[5]

[1] *California Institute of Technology[e], Pasadena, CA 91125, USA*

[2] *University of California at Santa Cruz[f], Santa Cruz, CA 95064, USA*

[3] *Carnegie-Mellon University[g], Pittsburgh, PA 15213, USA*

[4] *Cracow Institute of Nuclear Physics, PL-30055 Cracow, Poland*

[5] *Deutsches Elektronen Synchrotron DESY, D-W2000 Hamburg, Germany*

[6] *Universität Erlangen-Nürnberg[h], D-W8520 Erlangen, Germany*

[7] *INFN and University of Firenze, I-50125 Firenze, Italy*

[8] *Universität Hamburg, I. Institut für Experimentalphysik[i], D-W2000 Hamburg, Germany*

[9] *Harvard University[k], Cambridge, MA 02138, USA*

[10] *University of Nijmegen and NIKHEF[l], NL-6525 ED Nijmegen, The Netherlands*

[11] *Princeton University[m], Princeton, NJ 08544, USA*

[12] *Department of Physics[n], HEPL, and Stanford Linear Accelerator Center[o], Stanford University, Stanford, CA 94305, USA*

[13] *Universität Würzburg[p], D-W8700 Würzburg, Germany*

Abstract

Using the Crystal Ball detector at the e^+e^- storage ring DORIS II, we have measured the branching fraction to muon pairs $B_{\mu\mu}$ of the $\Upsilon(1S)$ and $\Upsilon(2S)$ resonances and for the first time the product of the muonic partial width $\Gamma_{\mu\mu}$ and the branching fraction to electrons B_{ee} for both resonances. We obtain

$$\begin{aligned} B_{\mu\mu}(1S) &= (2.31 \pm 0.12 \pm 0.10)\ \% \\ \Gamma_{\mu\mu}(1S)\cdot B_{ee}(1S) &= (31.2 \pm 1.6 \pm 1.7)\ \text{eV} \end{aligned}$$

and

$$\begin{aligned} B_{\mu\mu}(2S) &= (1.22 \pm 0.28 \pm 0.19)\ \% \\ \Gamma_{\mu\mu}(2S)\cdot B_{ee}(2S) &= (6.5 \pm 1.5 \pm 1.0)\ \text{eV}. \end{aligned}$$

Inserting the present world average value of $B_{ee}(1S) = (2.52 \pm 0.17)$ %, we determine the muonic partial width of the $\Upsilon(1S)$ as

$$\Gamma_{\mu\mu}(1S) = (1.24 \pm 0.06 \pm 0.11)\ \text{keV}.$$

In addition, we present the first indication of the expected interference between μ-pair production in the continuum and in $\Upsilon(1S)$ decays.

(Submitted to Zeitschrift fur Physik)

---

[a] Present Address: Max-Planck-Institut für Physik, D-W8000 München 40, Germany
[b] Permanent Address: DPHPE, Centre d'Etudes Nucléaires de Saclay, F-91191 Gif sur Yvette, France
[c] Permanent Address: CERN, CH-1211 Genève 23, Switzerland
[d] Permanent Address: Institute of Physics and Nuclear Techniques, AGH, PL-30055 Cracow, Poland

[e] Supported by the U.S. Department of Energy, contract No. DE-AC03-81ER40050 and by the National Science Foundation, grant No. PHY75-22980
[f] Supported by the National Science Foundation, grant No. PHY85-12145
[g] Supported by the U.S. Department of Energy, contract No. DE-AC02-76ER03066
[h] Supported by the German Bundesministerium für Forschung und Technologie, contract No. 054 ER 12P
[i] Supported by the German Bundesministerium für Forschung und Technologie, contract No. 054 HH 11P(7) and by the Deutsche Forschungsgemeinschaft
[k] Supported by the U.S. Department of Energy, contract No. DE-AC02-76ER03064
[l] Supported by FOM-NWO
[m] Supported by the U.S. Department of Energy, contract No. DE-AC02-76ER03072 and by the National Science Foundation, grant No. PHY82-08761
[n] Supported by the U.S. Department of Energy, contract No. DE-AC03-76SF00326 and by the National Science Foundation, grant No. PHY81-07396
[o] Supported by the U.S. Department of Energy, contract No. DE-AC03-76SF00515
[p] Supported by the German Bundesministerium für Forschung und Technologie, contract No. 054 WU 11P(1)

Introduction

The energy resolutions of today's e^+e^- colliders are about two orders of magnitude larger than the total widths of the three lowest Υ(nS) states (n=1,2,3). Thus, the total widths of these resonances can be obtained only from the ratio of their leptonic widths $\Gamma_{\ell\ell}$ to their leptonic branching fractions $B_{\ell\ell}$. Furthermore, a precise knowledge of $B_{\ell\ell}$ is needed to determine branching ratios for cascade decays between these resonances, since such decays are usually measured in exclusive final states where the lower lying resonance decays to a lepton pair. The measurement of $B_{\ell\ell}$ also provides a way to determine the strong coupling constant α_s and the QCD scale parameter Λ from a ratio of the Υ branching fraction to three gluons and the leptonic branching fraction [1], although the accuracy is limited by theoretical uncertainties [2] of higher order QCD corrections and by scale ambiguities.

In this paper we report measurements of $B_{\mu\mu}$ and $\Gamma_{\mu\mu}\Gamma_{ee}/\Gamma$ for the Υ(1S) and the Υ(2S) resonances. The data were collected with the Crystal Ball detector at the e^+e^- storage ring DORIS II in the years 1983 through 1986. The data samples represent integrated luminosities of 46 pb^{-1} on and around the Υ(1S), 37 pb^{-1} on and around the Υ(2S), and 72 pb^{-1} on and below the Υ(4S).

To measure $B_{\mu\mu}$ we use the excess of μ pairs on resonance compared to the continuum $e^+e^- \to \mu^+\mu^-$ production. The continuum μ-pair yield was derived from a Monte Carlo prediction, normalising it to the observed μ-pair cross section in the continuum data. The continuum data subsamples comprise 8 pb^{-1} below the Υ(1S), 2 pb^{-1} below the Υ(2S), and the complete sample of 72 pb^{-1} below and on the Υ(4S). The leptonic branching fraction of the Υ(4S) is small enough that the latter data can be regarded as continuum.

The value of $\Gamma_{\mu\mu}\Gamma_{ee}/\Gamma$ is obtained by fitting the observed cross section for $e^+e^- \to \mu^+\mu^-$ as a function of the e^+e^- center-of-mass (c.m.) energy W in the region of the respective resonance.

The paper is organised as follows. First, we briefly describe the detector and our Monte Carlo simulation, and present the determination of the c.m. energy and the luminosity for our data samples. Then we discuss the selection of μ-pair events and the background determination. In the next two sections $B_{\mu\mu}$ and $\Gamma_{\mu\mu}\Gamma_{ee}/\Gamma$ are obtained, and an indication of the interference of $\Upsilon(1S) \to \mu^+\mu^-$ with the continuum is presented. The concluding section summarizes our results and uses them to derive $\Gamma_{\mu\mu}$(1S).

The Experimental Setup

The Crystal Ball detector is described elsewhere [3, 4], and its properties are only briefly summarized here. Its main component is a nonmagnetic calorimeter consisting of a spherical

shell of 672 NaI(Tl) crystals covering 93% of 4π sr. Each crystal is about 16 radiation lengths deep, corresponding to about one nuclear interaction length. The arrangement is based on an icosahedron, in which each face, called "Major Triangle", is subdivided into four smaller triangles, called "Minor Triangles", which in turn are formed by the triangular faces of nine individual crystals. A complete sphere would contain 720 crystals. To allow entry and exit of the beams, 24 crystals are omitted on each side. The 30 crystals nearest to the beam pipe on each side are called "Tunnel Regions". The "Main Ball", used in the trigger and data analysis, excludes the Tunnel Regions and covers 84% of the solid angle. The overall solid angle coverage is increased to 98% by NaI(Tl) "Endcap Crystals".

The minimum energy recorded per crystal is 0.35 MeV. This small threshold together with the fine detector segmentation provides an ideal basis for recognizing different types of particle interactions in the calorimeter by their lateral energy distributions. Minimum ionization can be distinguished from electromagnetic showers or hadronic interactions by the fact that all but few percent of the energy deposition is contained in one or two crystals. The most probable energy loss in the crystals for minimum ionizing particles with $\beta\gamma$=4–5 is 195–200 MeV, and increases to 217 MeV at $\beta\gamma$=45 [5]. The width of the energy loss distribution is about 20 MeV, with some dependence on the particle momentum.

The central cavity of the detector is equipped with a set of tube chambers with charge division readout. The Υ(2S) data used in this analysis were taken with a chamber setup consisting of two double layers of proportional tubes and one double layer of streamer tubes, with a total number of 600 tubes. For the Υ(1S) and Υ(4S) data the streamer tubes have been replaced by two additional double layers of proportional tubes, resulting in a total of 800 tubes grouped in four double layers. Charged particles are detected with an efficiency of more than 98% for both setups. Their directions are determined by a fit through all tube hits assigned to the track and the position of the energy deposit in the ball. The resulting accuracy of the direction measurement is $2^\circ - 3^\circ$ in θ, the polar angle with respect to the beam axis, and better than 1° in φ, the azimuthal angle.

The time of flight system of the Crystal Ball detector has two parts. The "Ball-ToF" system consists of 20 TDCs, each processing the summed signals of one Major Triangle. The "Roof-ToF" system is a set of 94 scintillation counters located on the roof and on the side walls of the detector hut. It covers 25% of the solid angle and provides timing information for about 80% of the triggered cosmic ray events. The time of flight is measured at mean distances to the interaction point of 0.45 m by the Ball-ToF and 3.5 m by the Roof-ToF. Both measurements have a resolution of 1.0 ns for high energy muons, improving to 0.4 ns for the Ball-ToF measurement of high energy showering particles. With the help of the timing difference between the two components, cosmic ray events can be separated by about

14 standard deviations from e^+e^- annihilation events.

Muon pair events are efficiently recorded by two triggers, both of which rely entirely on the NaI(Tl) detector. One trigger requires two back-to-back Major Triangles, each having a deposited energy of more than 150 MeV; the other trigger requires at least 90 MeV in each of two back-to-back Minor Triangles. Both triggers are vetoed by energy depositions of more than 35 MeV in either Tunnel Region. Multi-hadron events are accepted with high efficiency by the Total Energy Trigger, which requires at least 1.8 GeV of energy deposited in the Main Ball.

Monte Carlo Simulations

The Monte Carlo simulation of the detector comprises three steps: the generation of particle 4-vectors, the simulation of the detector response, and the reconstruction of the simulated events, as discussed below.

For generating μ-pair events from e^+e^- annihilation we use the DYMU2 program [6], which includes initial state photon radiation to order α^2, and final state photon radiation to order α^1. A structure function approach [7] is used to exponentiate the initial and final state photon spectra to all orders of α. Since the generator is written for the Z peak, it uses an approximation for the effect of vacuum polarization in the photon propagator that is not valid at our c.m. energies. To utilize the generator in the energy region of the Υ resonances, we have made several modifications [8]. We account for the vacuum polarization by including the one-loop amplitude and its iterations in a "chain sum". The leptonic part of the vacuum polarization is implemented by an analytical correction to the annihilation cross section. The hadronic part is handled numerically using results from a fit to a detailed calculation for quark loops [9], including all narrow resonances below the Υ. In addition, the effects of all Υ resonances have been explicitly taken into account as given in Ref. [10]. The modifications include all interference terms among the lowest order amplitude, the vacuum polarization, and the Υ resonance terms. Finally, the e^+e^- c.m. energy spread w has been included. The modified generator is employed for several purposes, namely for predicting the observed continuum cross section from $e^+e^- \rightarrow \mu^+\mu^-$, for deriving the selection efficiency for resonance decays to muons, for calculating the interference contribution between resonant μ pairs and those from continuum production, and for fitting the μ-pair cross section in the resonance regions. These different modes of application are described in later sections.

The detector response to all particles except electrons and photons has been simulated by an upgraded version [5] of the GHEISHA 6/7 program [11]. Among other modifications, corrections in the modeling of energy loss and of δ-electrons have been applied. They have been proven to be important for a realistic simulation of particle interactions, which is

essential for this analysis. The energy depositions of electromagnetically showering particles, including secondary particles like δ-electrons, are simulated by the EGS 3 program [12]. The pulse height distributions of the tube chamber hits, their efficiency, and the resolution of the charge division readout, including their respective run-dependences, are modeled by a separate Tube Chamber Monte Carlo program [8]. The Ball-ToF was simulated by a Gaussian distribution with mean value and width determined from the data. The Roof-ToF was not simulated, since it was used only as a veto against cosmic rays. Its rejection rate for collision events is far below 0.1%. Extra energy in the ball and additional hits in the tube chambers originating from beam-related background are taken into account by overlaying special background events onto the Monte Carlo events. Those background events are obtained by triggering on every 10^7th beam crossing, with no other condition.

The Monte Carlo events were then reconstructed and subjected to the same cuts as the real data.

Determination of the Center-of-Mass Energy

For the Υ(1S) and Υ(2S) data, multi-hadron events are used to derive the number of produced Υ resonances and to determine the e^+e^- c.m. energy W. They are selected with cuts identical to those from Ref. [4]. The selection criteria are well suited to suppress background from beam-gas and beam-wall reactions, two-photon collisions, and QED processes like e- and τ-pair production. The resulting samples comprise 447×10^3 and 253×10^3 multi-hadron events from the Υ(1S) and Υ(2S) data, respectively.

At DORIS II the distribution of the e^+e^- c.m. energy $\sqrt{s}$ follows a Gaussian of width $w \approx 8$ MeV (see Table 1) around a mean value W. A precise knowledge of W is required for fitting the μ-pair cross section in the resonance region as a function of W, and for the measurement of $B_{\mu\mu}$. The latter can be seen from the expression for the lowest order cross section σ_0 for $e^+e^- \to \mu^+\mu^-$ including a resonance of mass M [10]

$$\sigma_0 = \frac{4\pi\alpha^2}{3s}\left(1 + 2\frac{\sqrt{9\Gamma_{\mu\mu}\Gamma_{ee}}}{\alpha M}\frac{s(s-M^2)}{(s-M^2)^2+M^2\Gamma^2} + \frac{9\Gamma_{\mu\mu}\Gamma_{ee}}{\alpha^2M^2}\frac{s^2}{(s-M^2)^2+M^2\Gamma^2}\right). \quad (1)$$

The first term in the parentheses denotes the continuum cross section $e^+e^- \to \mu^+\mu^-$, the last term describes the resonant μ-pair production $e^+e^- \to \Upsilon \to \mu^+\mu^-$, and the second term is the interference between them. The interference term has maximum values of $\pm4\pi\alpha\sqrt{B_{\mu\mu}B_{ee}}/M^2$ at $s = M(M \pm \Gamma)$, whereas the peak value of the resonance at $s = M^2$ is $12\pi B_{\mu\mu}B_{ee}/M^2$. The ratio of the maxima of these terms is thus $\alpha/\sqrt{9B_{\mu\mu}B_{ee}}$, yielding about 1/10 for the Υ(1S) and about 1/5 for the Υ(2S). These values do not change much after including radiative corrections and a convolution with the c.m. energy spread w. Shifting

W by only $w/3 \approx 2.7$ MeV from the peak of the resonance would decrease the observed hadronic cross section by only 4% on the $\Upsilon(1S)$ and by 3% on the $\Upsilon(2S)$, which could easily be overlooked during data taking. However, the same energy changes, due to the effect of interference, cause changes in the ratio of resonant μ-pair to resonant hadronic cross section of 5% for the $\Upsilon(1S)$ and 10% for the $\Upsilon(2S)$. To reduce resulting errors in the muonic branching ratio, which is calculated from the ratio of both cross sections, we carefully determine the c.m. energy for all data taken on either resonance.

For all of our $\Upsilon(1S)$ data and most of our $\Upsilon(2S)$ data, the magnetic field B at the beam position in a storage ring bending magnet was measured using the nuclear magnetic resonance effect (NMR). The conversion factor between W and B was obtained [8] by fitting the observed hadronic cross section as a function of B with the Υ-resonance curves, where the accepted Υ masses [13] were assumed. The conversion factor was the only free parameter in the fit. It was found that the conversion factor was not a constant in time, but sometimes jumped to a new value due to changes in the beam orbits. The fits were performed for periods of un-interrupted DORIS running, so that the conversion factor is expected to be constant within each period. Periods adjacent in time were combined if they could be consistently described by a common fit. The $\Upsilon(2S)$ data could be consistently fitted with a single conversion factor, whereas we got a set of 5 different conversion factors for the $\Upsilon(1S)$ data. They correspond to shifts ranging from 6.5 MeV to 44.2 MeV compared to those c.m. energy values which would have been obtained by utilizing the $\Upsilon(2S)$ conversion factor. From the errors of the fits and from the variation of the results within the sets of combined subperiods, we derive an error of $\Delta W = 0.5$ MeV on our determination of W.

A subset of 8 pb^{-1} of the $\Upsilon(2S)$ data was collected before a regular NMR reading existed at DORIS. Their c.m. energies were determined by exploiting resonance depolarization measurements [14, 15] with a resulting precision ΔW ranging from 0.5 MeV to 2.0 MeV [8].

A precise determination of W for the $\Upsilon(4S)$ data is not necessary, since the muons from $\Upsilon(4S)$ decays change the observed continuum μ-pair cross section by at most 0.3%. Thus the c.m. energy of the $\Upsilon(4S)$ on-resonance data was set equal to the $\Upsilon(4S)$ mass from Ref. [13], accounting for possible offsets by an error of $\Delta W = 15$ MeV. The c.m. energies of the continuum data below the $\Upsilon(4S)$ were calculated from their c.m. energy difference to the $\Upsilon(4S)$ resonance data. This difference was deduced from the magnet's currents, allowing for an error of $\Delta W = 20$ MeV.

For the analysis we assemble data sets of constant c.m. energy W by collecting data with nearby values of W from all periods, and assigning to each data set a luminosity weighted average c.m. energy $W_i = \sqrt{\sum \mathcal{L} W^2 / \sum \mathcal{L}}$. We end up with 28 data sets of different c.m. energies around the $\Upsilon(1S)$, 13 data sets around the $\Upsilon(2S)$, and 4 data sets on and below

the $\Upsilon(4S)$, as shown in Fig. 1(a).

Luminosity Determination

The integrated luminosity $\mathcal{L}$ is determined with the help of events from the processes $e^+e^- \to e^+e^-$ and $e^+e^- \to \gamma\gamma$. They are selected by requiring exactly two clusters in the calorimeter with a deposited energy of $E_{cluster} > 0.7E_{\rm beam}$. Both clusters have to lie within $|\cos\theta| < 0.75$, where the directions are determined not from the tracks in the chambers, but from the energy depositions in the ball with respect to the ball's center. The observed cross sections have been computed with the event generators of Ref. [16] and our detector simulation. The simulation predicts the selected luminosity events to be composed of about 11% $e^+e^- \to \gamma\gamma$ events and 89% Bhabha events. Background from sources like $e^+e^- \to \tau^+\tau^-$ or $e^+e^- \to q\bar{q}$ is below 0.2%. More details can be found in Ref. [17].

The systematic error on the luminosity measurement is 2.5% [15, 17]. For on-resonance data we correct the luminosity for the contribution from $\Upsilon \to e^+e^-$. Right on the resonance peaks the correction amounts to $-(1.30 \pm 0.15)\%$ for the $\Upsilon(1S)$ and to $-(0.35 \pm 0.10)\%$ for the $\Upsilon(2S)$. The systematic errors on this subtraction arise from the uncertainty in the Υ branching ratios to e^+e^-, and from uncertainties in the radiative corrections to the resonance peak heights and to the e^+e^- continuum. We further correct the luminosity for the dependence of the selection efficiency on the length l of the intersection region of the e^+e^- beams along the beam axis. Variations in l change the effective solid angle covered by our cut of $|\cos\theta| < 0.75$. From Monte Carlo studies simulating the angular distributions of luminosity events and the variation of l with time, as measured in Ref. [17], we find corrections ranging from -0.5% to +0.3%. For about 40% of our $\Upsilon(1S)$ data the measured luminosity had to be increased by $(2.7\pm0.3)\%$ to compensate a nonlinear performance of the electronic crystal readout [17].

μ-Pair Event Selection

The μ-pair events were selected by applying the following cuts based on calorimeter, ToF, and chamber information:

- There are two energy depositions in the Main Ball fulfilling the requirements of both the Major and the Minor Triangle Trigger, with software thresholds at 160 MeV and 120 MeV, respectively, and less than 30 MeV in each Tunnel Region.
- Each energy deposition is smaller than 400 MeV, and the total energy deposited in the Main Ball plus Tunnel Regions plus Endcaps is less than 1000 MeV.

- More than 94.5% of each energy deposition is contained in two adjacent crystals.
- Additional energy in the ball, including the Tunnel Regions, is less than 30 MeV.
- At least one of the two energy depositions in the ball has associated hits in the tube chambers.
- The particle directions are back-to-back within a cone of 12 degrees.
- The tracks are consistent with coming from the beam axis.
- Averaging over both particles, the energy loss in the proportional tube chambers plotted versus the inverse particle velocity, as measured by the Ball-ToF with respect to the bunch crossing time, is consistent with the expectation for annihilation μ pairs.
- For particles associated with a Roof-ToF hit, the time difference to the Ball-ToF measurement is more than 4 standard deviations from the value expected for cosmic rays.

After the selection we have 26.6×10^3, 17.5×10^3, and 31.9×10^3 μ-pair candidate events on and around the $\Upsilon(1S)$, $\Upsilon(2S)$, and $\Upsilon(4S)$, respectively. To extract the number of $\Upsilon(1S)$ and $\Upsilon(2S)$ resonance decays to μ pairs from this event sample, we have to subtract the contribution from the continuum process $e^+e^- \rightarrow \mu^+\mu^-$ together with other background. This other background is due to two-photon reactions $e^+e^- \rightarrow e^+e^-\mu^+\mu^-$, $e^+e^-\pi^+\pi^-$, $e^+e^-e^+e^-$, leptonic decays of τ pairs from $e^+e^- \rightarrow \tau^+\tau^-$, cosmic ray events, and eN interactions of beam electrons with nuclei in the wall of the beam pipe or in the residual gas. The applied selection criteria are designed to suppress these background contributions as described below.

Cosmic ray background is efficiently reduced by the selection criteria based on chamber and timing information. Nearly all cosmic ray tracks that pass the beam line with an impact parameter of larger than about 1 cm are inconsistent with coming from the beam axis. All cosmic rays that intersect the Roof-ToF counters are rejected with the help of the timing difference between Roof- and Ball-ToF. The calculation of the inverse particle velocity from the Ball-ToF with respect to the bunch crossing signal results in a flat distribution for cosmic ray events, because they have no correlation with the bunch crossing time. The remaining background from cosmic rays is thus observed as a horizontal band in the distribution of average energy loss in the proportional tube chambers versus inverse particle velocity. From the sidebands in this distribution a residual cosmic ray background of typically 2% was determined separately for each of our data sets and subtracted from the observed numbers of events.

Our cut in the plane of the average energy loss in the tube chambers versus the inverse particle velocity rejects some events at large energy losses and low velocities, consistent with values expected for protons. To study their origin, we examine a sample of μ-pair candidate events where some of the cuts have not been applied. In this sample we find for most of the "proton" events vertices in the wall of the beam pipe. Thus we can attribute them mainly to the reaction of a beam electron with a nucleus in the wall of the beam pipe, eN $\rightarrow$ ppX. We find that almost all cuts on calorimeter, chamber, and ToF information are effective against this background. For estimating the residual background from eN events, we select two independent eN samples from our μ-pair candidate events by requiring an event vertex in the wall of the beam pipe for the first one, and large energy loss together with low particle velocity for the second one. From the first sample we obtain the distribution of eN events in the plane of energy loss versus velocity, and from the second sample their vertex distribution. With the help of each distribution, we estimate the residual eN background from the numbers of events rejected when the respective cut is applied at the very end of the selection [8]. Both methods consistently yield estimates of about 0.1%, slightly varying among the different data sets. These estimated numbers of eN events are added to the e^+e^- backgrounds calculated in the following section.

The two-photon background and the contamination from τ-pair events are strongly suppressed by the requirements on the particle directions and the amounts of deposited energy. Particle pairs from these sources are in general not back-to-back. In most events from two-photon interactions at least one of both particles is produced with a kinetic energy below 160 MeV. On the other hand, electrons and pions from τ decays deposit in most cases more than 400 MeV in the calorimeter. Those final states from two-photon or τ-pair production that contain electrons are essentially completely rejected by the cut on the lateral energy distributions, since their electromagnetic showers are spread over more than only two crystals. As will be discussed in the next section, the remaining background from the above sources is a function of the c.m. energy and ranges from 20% to 26% of the predicted continuum background from $e^+e^- \rightarrow \mu^+\mu^-$. It is dominated by the process $e^+e^- \rightarrow e^+e^-\mu^+\mu^-$.

Background Determination

In the $\mu^+\mu^-$ final state the Υ resonances rise only marginally above the continuum background from $e^+e^- \rightarrow \mu^+\mu^-$. The main task of our analysis is thus a precise determination of the background. This background will then be subtracted from the total observed μ-pair cross section.

In Fig. 1(a) we have plotted $\sigma_i^{\mu\mu}$, the observed μ-pair cross section after our selection, for each of the 45 values W_i. The cosmic ray events have already been subtracted as described

in the preceding section. The dotted lines show the behaviour of the observed cross section that would be expected if the detector acceptance were constant in time. We observe significant point-to-point variations deviating by typically 10% from such a smooth cross section. These variations are due to changes in the detector acceptance, induced for example by variations in the amount of beam-related extra energy deposits, variations in the tube chamber performance, and variations in the position of the e^+e^- interaction region and in its spread along the beam axis.

For subtracting the continuum background we have to know precisely its point-to-point fluctuations as well as its mean amplitude. A Monte Carlo detector simulation is used to predict the background from e^+e^- interactions. Its mean amplitude is checked by comparing the prediction for six off-resonance c.m. energies with the corresponding data, as detailed later. The Monte Carlo simulation includes point-to-point fluctuations of the observed cross section by modeling time dependent variations of the detector acceptance for each c.m. energy W_i. Beam-related background signals from samples of more than 1000 background events per day of running have been overlayed onto the simulated raw data of each event, tube chamber parameters have been determined typically for each two days of running, and variations in the length and position of the e^+e^- intersection region have been simulated as measured in Ref. [17], averaged over appropriate periods. For the two most prominent backgrounds, the continuum μ-pair production $e^+e^- \to \mu^+\mu^-$ and the two-photon process $e^+e^- \to e^+e^-\mu^+\mu^-$, we simulate each of the 45 data sets separately. For the less prominent background sources ($e^+e^- \to \tau^+\tau^-$ and two-photon production of $\pi^+\pi^-$ and e^+e^-) we generate three Monte Carlo samples combined for all energies around the Υ(1S), Υ(2S), and Υ(4S), respectively.

The prediction for the observed continuum cross section has been obtained by simulating the detector response to $e^+e^- \to \mu^+\mu^-$ events generated by the DYMU2 program. For producing events around the Υ(1S), Υ(2S), and Υ(4S), the corresponding resonance amplitude (and thus also its interference terms) was removed from the cross section calculation. However, to properly simulate the c.m. energy dependence of the background cross section, we have included all resonance and interference terms from the other Υ resonances. Events around the Υ(2S) were simulated with a transverse beam polarization of 75%, as observed in the data [14].

The two-photon contribution to the observed continuum cross section was determined using the event generators of Refs. [18, 19, 20] and our detector simulation. As a function of the c.m. energy the contributions from $e^+e^- \to e^+e^-\mu^+\mu^-$, $e^+e^- \to e^+e^-\pi^+\pi^-$, and $e^+e^- \to e^+e^-e^+e^-$ range from 18% to 24%, from 1.4% to 1.9%, and from 0.15% to 0.19%, respectively, all given in terms of the predicted continuum background from $e^+e^- \to \mu^+\mu^-$. The contribution from $e^+e^- \to \tau^+\tau^-$ events amounts to 0.45% of this cross section, where

the events have been simulated according to Ref. [21].

Fig. 1(b) shows the prediction for the continuum background cross section σ_i^{BG} for each of our 45 c.m. energies W_i. It has been obtained by summing the Monte Carlo predictions for the e^+e^- background and the estimation of the eN background from above. Like the data in Fig. 1(a), this prediction also reveals significant point-to-point variations. In the following we study the mean amplitude of this prediction as well as its ability to reproduce the point-to-point variations of the background.

To check the mean amplitude, we compare the observed cross section $\sigma^{\mu\mu}$ (Fig. 1(a)) and the background prediction σ^{BG} (Fig. 1(b)) by defining a scaling factor

$$C \equiv \left\langle \frac{\sigma_j^{\mu\mu}}{\sigma_j^{BG}} \right\rangle_{\rm off} . \tag{2}$$

In the calculation of this average, each point is weighted by its error, and the average is taken over the off-resonance c.m. energies W_j. Since $\sigma_j^{\mu\mu}$ should be equal to σ_j^{BG} off resonance, the resulting value of C should be 1 within its systematic error of 3.5%, which arises to equal parts from our luminosity measurement and from the error on σ^{BG} [8]. This represents a crucial consistency check of our analysis.

In addition, using this scaling factor considerably reduces our systematic error on the background subtraction. By multiplying each point of the background prediction with the same factor C, obtained from Eq. (2), we fix the mean amplitude of the subtracted background to that level which has been observed in the data. The main systematic error on the background subtraction then arises from the reproduction of the point-to-point variations. This can be seen by rewriting Eq. (2) as

$$C \approx \frac{N_{\rm off}^{\mu\mu}}{\mathcal{L}_{\rm off}\sigma_{\rm off}^{BG}}, \tag{3}$$

where $N_{\rm off}^{\mu\mu}$ is the number of observed μ-pair events summed over the off-resonance c.m. energies, $\mathcal{L}_{\rm off}$ is the sum of the corresponding luminosities, and $\sigma_{\rm off}^{BG} \equiv \langle \sigma_j^{BG} \rangle_{\rm off}$ is the mean predicted off-resonance (background) cross section. We obtain the observed number $N_i^{\Upsilon\to\mu\mu}$ of resonance decays to muons for each W_i from

$$N_i^{\Upsilon\to\mu\mu} = N_i^{\mu\mu} - C\mathcal{L}_i\sigma_i^{BG} \tag{4}$$

$$\approx N_i^{\mu\mu} - N_{\rm off}^{\mu\mu}\frac{\mathcal{L}_i}{\mathcal{L}_{\rm off}}\frac{\sigma_i^{BG}}{\sigma_{\rm off}^{BG}}, \tag{5}$$

where $N_i^{\mu\mu}$ is the number of observed μ-pair events at each W_i. This way of background subtraction does not depend on the absolute values of $\mathcal{L}_i$ and σ_i^{BG}. Their systematic errors are thus eliminated. Instead we see from Eq. (5) that now the errors on the *ratios* $\mathcal{L}_i/\mathcal{L}_{\rm off}$

and $\sigma_i^{BG}/\sigma_{\rm off}^{BG}$ as well as the error on the measured number $N_{\rm off}^{\mu\mu}$ are relevant. These errors are all smaller than the 2.5% uncertainties of $\mathcal{L}_i$ and σ_i^{BG} alone.

In the following we first determine the value of C and then investigate the errors on the luminosity ratios and on the ratios of the background predictions. Special emphasis has been given to a thorough calculation of both errors. Since we subtract in Eq. (4) two large numbers from each other, an error on the subtracted background $N_i^{BG} \equiv C\mathcal{L}_i\sigma_i^{BG}$ has a strong impact on the result for $N_i^{\Upsilon\to\mu\mu}$. Fractional errors on $\mathcal{L}_i/\mathcal{L}_{\rm off}$ and $\sigma_i^{BG}/\sigma_{\rm off}^{BG}$ cause a fractional error on the number $N_i^{\Upsilon\to\mu\mu}$ which is larger by a factor of $\lambda = N_i^{BG}/N_i^{\Upsilon\to\mu\mu}$. Summing over c.m. energies W_i within ± 10 MeV of the resonance peaks in Fig. 1(a), we find the values $\lambda(1S)=4.8$ and $\lambda(2S)=23$.

We determine C from Eq. (2) by averaging over 6 off-resonance points, using the data sets of 8 pb^{-1} at the lowest continuum c.m. energy below the Υ(1S), 2 pb^{-1} at the lowest continuum c.m. energy below the Υ(2S), and 9 pb^{-1}, 3 pb^{-1}, 4 pb^{-1}, and 57 pb^{-1} at the c.m. energies below and on the Υ(4S). As already mentioned in the introduction, the muonic branching ratio of the Υ(4S) is small enough that the latter data can be regarded as continuum. A fit of a constant C to the ratios $\sigma^{\mu\mu}/\sigma^{BG}$ for these 6 points has a confidence level of 44% and results in

$$C = 0.999 \pm 0.006.$$

The error of this number is dominated by the data statistics. It contains in addition small contributions from Monte Carlo statistics, from the statistics of luminosity events, and from the Υ(4S) interference with the continuum as discussed below. The fit result shows that our prediction for the amplitude of the observed cross section is in excellent agreement with the off-resonance data.

For the estimation of the errors on the luminosity ratio and on the ratio of the background prediction, we study in the following all effects that potentially could introduce variations of more than 0.1% in the detector acceptance or the amount of background.

The luminosity ratio is affected by several factors: (1) a variation of the $\cos\theta$ acceptance for luminosity events due to the variation of the bunch length with time, (2) the nonleading energy dependence of the Bhabha cross section, (3) the amount of $\Upsilon \to e^+e^-$ decays contributing to the number of observed electron pairs on resonance, (4) a period of nonlinear performance of the electronic crystal readout in the Υ(1S) data [17, 22], and (5) the statistics of luminosity events. We find a combined error of 0.2% for $\mathcal{L}_i/\mathcal{L}_{\rm off}$, which has been reduced to this small value by explicitly correcting for all systematic influences listed. The residual error reflects the accuracy of our corrections together with the combined statistical error for all points on either resonance.

The systematic error on $\sigma_i^{BG}/\sigma_{\rm off}^{BG}$ has contributions from uncertainties in the cross section

dependence on W, from inaccuracies in reproducing variations of the detector acceptance, and from Monte Carlo statistics. The three sources combine to an error of 0.6%. We will discuss each contribution in turn.

The first item covers the genuine variations of the background cross section with W, which are not due to detector acceptance effects. We find a combined error of 0.2% from the following sources: (1) the uncertainty in $\sigma^{ee\to\mu\mu}(W)$, which is dominated by uncertainties in the interference term of the (rare) decay $\Upsilon(4S)\to\ \mu^+\mu^-$ with the continuum due to the error of 15 MeV on the c.m. energy of the on-$\Upsilon(4S)$ data, (2) the uncertainty in the W dependence of the other e^+e^- background processes, dominated by that of $\sigma^{ee\to ee\mu\mu}(W)$, (3) the calculation of the variation of the residual background from eN events with W, and (4) possible differences in the scaling factor C for the different background sources, which would lead to a dependence of C on W.

The accuracy of the Monte Carlo in reproducing our time-dependent acceptance for the background processes from e^+e^- interactions has been determined to be 0.4%. The main sources of this error are the accuracy in modeling the variations in time of the bunch length of the beam, and possible variations of the width of the energy loss distribution due to variations in the detector calibration. Other contributions to this systematic error are the accuracy in modeling the variations of the beam position, of the chamber resolution, and of the beam-related extra energy deposits, and possible variations in the size of the air gap between the upper and the lower ball hemisphere. The trigger efficiencies do not significantly contribute to this error, because our software thresholds have been chosen such that the efficiencies generally are undistinguishable from 100.0%. Exceptions are 13 pb^{-1} of $\Upsilon(1S)$ data, where only the Major Triangle Trigger was enabled, resulting in $\epsilon_{trig} = (99.7 \pm 0.1)\%$ and 8 pb^{-1} of $\Upsilon(2S)$ data, where two Minor Triangles were not properly included in both triggers, resulting in $\epsilon_{trig} = (97.2 \pm 0.2)\%$.

Finally, the Monte Carlo statistics on $\sigma_i^{BG}/\sigma_{\rm off}^{BG}$ contribute an error of 0.4%, which is a factor of 2.5 less than the corresponding statistical error from the data.

The error on $\sigma_i^{BG}/\sigma_{\rm off}^{BG}$ together with the error on $\mathcal{L}_i/\mathcal{L}_{\rm off}$ means that we should be able to reproduce the observed point-to-point variations of $\sigma^{\mu\mu}(W_i)$ in Fig. 1(a) with a precision of 0.7%. Given point-to-point variations of $\mathcal{O}(10\%)$, this is a remarkably high precision, which is mainly owing to our run-dependent Monte Carlo simulation of beam-related extra energy deposits, of length and position of the e^+e^- intersection region, and of the chamber performance. To derive the influence of this error on $N^{\Upsilon\to\mu\mu}$, the observed number of resonance decays to muons, we have to multiply it with the factors $\lambda(n\mathrm{S})$ determined above. This results in errors of 3.2% for the $\Upsilon(1S)$ and 15% for the $\Upsilon(2S)$, which are the dominant systematic errors in our analysis (cf. Table 3).

The high precision of our point-to-point background prediction is supported by the good confidence level in fitting the constant C to 6 different data points and by the good correlation of the variations of the high statistics points around the dotted lines in Fig. 1 between the data (a) and the background prediction (b). This correlation is confirmed by our final fits to the background subtracted cross section (Figs. 2(b) and 3(b)), which have confidence levels of 99% and 65%, respectively.

Determination of $B_{\mu\mu}$

The μ-pair branching ratios $B_{\mu\mu}$ for the Υ(1S) and the Υ(2S) are derived by dividing the number of resonant μ pairs by the total number of produced Υ resonances. In this ratio we have to account for the fact that the cross section for resonance decays to muons and the total number of produced Υ decays are differently affected by the interference of resonance and continuum. Only decays to fermion pairs, namely $\Upsilon \to q\bar{q}$ and $\Upsilon \to \ell\bar{\ell}$, interfere with non-resonant continuum production, whereas for all other Υ decays, such as $\Upsilon(2S) \to \pi\pi + \Upsilon(1S)$ or $\Upsilon \to ggg$, there is no or negligible interference with the continuum. For each c.m. energy W_i we correct the cross section of resonance decays to μ pairs by the interference term σ_i^I and the Υ production cross section by $(3 + R)\sigma_i^I$. The factor 3 accounts for the three leptonic decay modes and R, the ratio of the hadronic continuum cross section to the Born cross section for μ-pair production, relates the $q\bar{q}$ decay of the Υ to its leptonic decays. The value of σ_i^I mainly depends on $\sqrt{\Gamma_{\mu\mu}\Gamma_{ee}}$ and on the c.m. energy spread w. It was calculated from the modified DYMU2 generator as the difference between the cross sections generated with and without interference, inserting $\Gamma_{\mu\mu} = \Gamma_{ee}$ from [13], and w as measured below.
We then obtain $B_{\mu\mu}$ from

$$B_{\mu\mu} = \frac{\sum_i \left(\frac{N_i^{\Upsilon \to \mu\mu}}{\varepsilon_i^{\Upsilon \to \mu\mu}} - \mathcal{L}_i \sigma_i^I \right)}{\sum_i \left(\frac{N_i^{\Upsilon \to \mathrm{had}}}{\varepsilon_i^{\Upsilon \to \mathrm{all}}} - \mathcal{L}_i (3 + R) \sigma_i^I \right)}, \tag{6}$$

where i runs over all c.m. energies W_i within 10 MeV of the resonance peak, $N_i^{\Upsilon \to \mu\mu}$ is the number of observed Υ decays to muons, $\varepsilon_i^{\Upsilon \to \mu\mu}$ is their detection efficiency, $\varepsilon_i^{\Upsilon \to \mathrm{all}}$ denotes the acceptance of our multi-hadron selection for *all* Υ decays, and $N_i^{\Upsilon \to \mathrm{had}}$ is the observed number of Υ decays to hadrons.

We evaluate $N_i^{\Upsilon \to \mathrm{had}}$ by subtracting the continuum contribution from the total number N_i^{had} of multi-hadron events observed at each c.m. energy W_i according to

$$N_i^{\Upsilon \to \mathrm{had}} = N_i^{\mathrm{had}} - \mathcal{L}_i \sigma^{ee \to qq}(W_i), \tag{7}$$

where the observed continuum cross section $\sigma^{ee\to qq}(W_i)$ has been fitted in the region of the resonances (see Figures 2(a), 3(a), and Table 1). This results in a total number of observed hadronic Υ decays of $(272.3 \pm 1.0)\times10^3$ and $(110.4 \pm 1.7)\times10^3$ for the Υ(1S) and the Υ(2S), respectively, where the errors are statistical only.

To obtain the total number of produced Υ decays, we have to divide $N_i^{\Upsilon\to had}$ by the fraction $\varepsilon_i^{\Upsilon\to all}$ of all Υ decays that pass our multi-hadron selection. This fraction is calculated from the relative abundance of all Υ decay channels, including the leptonic channels with a branching ratio equal to our final $B_{\mu\mu}$ number, together with the efficiency of the multi-hadron selection for each channel. The branching ratio of the $q\bar{q}$ channel has been derived from $B_{qq} = RB_{\mu\mu}$, where R has been taken from Ref. [15]. The detection efficiency for hadronic Υ decay modes has been determined using the LUND event generators [23] and our detector simulation. Since the relative abundances of Υ decays are influenced by the interference effects, the efficiency $\varepsilon_i^{\Upsilon\to all}$ varies with the c.m. energy from 85.7% to 88.5% for the Υ(1S) decays, and from 87.3% to 89.8% for the Υ(2S) decays. The mean efficiencies, averaged over the resonance regions, are (87.1 ± 1.2)% for the Υ(1S) decays, and (88.5 ± 1.5)% for the Υ(2S) decays, where the systematic errors arise mainly from the hadronization model dependence, from uncertainties in the detector response to hadrons, and from the error on our final $B_{\mu\mu}$ value.

Furthermore we subtract the interference effects of $\sum \mathcal{L}_i(3+R)\sigma_i^I = (-0.5 \pm 0.5)\times10^3$ and $(-0.2 \pm 0.2)\times10^3$ from the number of produced Υ(1S) and Υ(2S) decays, respectively. The interference correction is very small because only the fermionic Υ decays contribute and the interference effects below and above the resonance essentially cancel (see below). This correction increases the total number of produced resonances to the final values of $(313.2 \pm 1.1 \pm 4.4)\times10^3$ Υ(1S) resonances and to $(125.0 \pm 1.9 \pm 2.1)\times10^3$ Υ(2S) resonances. The systematic errors on these values arise mainly from the errors on the efficiency $\varepsilon^{\Upsilon\to all}$, as discussed above.

The number of observed resonance decays to muons, $N_i^{\Upsilon\to\mu\mu}$, in the numerator of Eq. (6) is obtained by subtracting the continuum background from the total number $N_i^{\mu\mu}$ of observed μ-pair events according to Eq. (4). A small resonant background arises from nonexclusive muonic resonance decays $\Upsilon \to \mu\mu$+X, namely from decays to τ pairs and from cascade decays from the Υ(2S) to the Υ(1S), where the Υ(1S) subsequently decays to a μ pair. Its amount was deduced from a Monte Carlo simulation of these channels. After subtraction of continuum and resonant background, we are left with $3189 \pm 162 \pm 104$ Υ(1S) resonance decays to muons and with $657 \pm 154 \pm 101$ μ-pair events from Υ(2S) resonance decays, as listed in Table 2. The systematic errors reflect the errors on $\mathcal{L}_i/\mathcal{L}_{off}$ and $\sigma_i^{BG}/\sigma_{off}^{BG}$ as discussed in the preceding section. We have to correct these numbers by the detection

efficiency and the interference contribution.

The selection efficiency for μ pairs from resonance decays has been determined for each c.m. energy W_i separately. The dependence of $\varepsilon^{\Upsilon\to\mu\mu}$ on W is twofold. First, there is the time-dependence of the detector acceptance, as discussed above. Second, there is a genuine dependence on W_i since initial state radiation leads to resonance production only for a limited range of photon energies. For the efficiency determination we used Monte Carlo events from the DYMU2 generator, where the energy range of the initial state photons was restricted depending on the distance in W from the respective resonance. Note that the final state photons have to be generated over their complete energy spectrum, since $B_{\mu\mu}$ is defined as the branching ratio to $\mu^+\mu^-$ plus an arbitrary number of photons with arbitrary energies. Since our μ-pair selection is very sensitive to additional photons in the event, our selection efficiency is lowered by $\sim$10% due to final state radiation. Averaged over each resonance the detection efficiencies are 44.6% and 44.1% for the Υ(1S) and Υ(2S), respectively. We assign a systematic error of 1.1% to these efficiencies. This error was estimated from a comparison of data with Monte Carlo distributions for all variables used in our selection cuts, and from the differences in energy and angular distributions for final state photons between the Monte Carlo generators DYMU2 [6] and MMG1 [24].

Given our systematic error in W, we are able to determine the interference corrections with precisions of about 1% and 2% of the number of Υ(1S) and Υ(2S) decays to muons, respectively. The net interference correction, however, is not significantly different from zero, because we selected the data in a symmetric range of 10 MeV around the resonances, thus canceling out most of the interference effect (see Table 2). Omitting a precise determination of W_i, on the other hand, the distribution of the c.m. energies with respect to the resonance peak would have been unknown, and the thus undetermined interference contribution would have led to additional systematic errors of $\sim$10%.

After these corrections, we end up with a total number of resonant μ pairs of $(7.22 \pm 0.36 \pm 0.30)\times10^3$ and $(1.52 \pm 0.35 \pm 0.23)\times10^3$ for the Υ(1S) and Υ(2S), respectively. Dividing these numbers by the corresponding numbers of produced resonances, we obtain for the two lowest lying Υ states values of

$$B_{\mu\mu}(1S) = (2.31 \pm 0.12 \pm 0.10)\%,$$

and

$$B_{\mu\mu}(2S) = (1.22 \pm 0.28 \pm 0.19)\%.$$

Table 2 summarizes the essential numbers for these measurements, and Table 3 gives the fractional influences of the various error sources.

Determination of $\Gamma_{\mu\mu}\Gamma_{ee}/\Gamma$

The quantity $\tilde{A}\equiv\Gamma_{\mu\mu}\Gamma_{ee}/\Gamma$ is proportional to the area A under the measured excitation curve $\sigma(W)$ of the Υ resonances in the process $e^+e^- \to \Upsilon \to \mu^+\mu^-$ through

$$\tilde{A} \equiv \frac{\Gamma_{\mu\mu}\Gamma_{ee}}{\Gamma} = \frac{1}{6\pi^2} M_\Upsilon^2 A. \tag{8}$$

$\tilde{A}$ can thus be obtained from a fit to the measured cross section $\sigma^{ee\to\Upsilon\to\mu\mu}(W)$ as shown in Figs. 2(b) and 3(b). This cross section has been obtained by subtracting from the observed μ-pair cross section of Fig. 1(a) the continuum background prediction of Fig. 1(b), scaled with $C = 0.999$, plus the small resonant background from nonexclusive muonic resonance decays. The resulting spectra have been corrected point-by-point with the detection efficiencies $\varepsilon_i^{\Upsilon\to\mu\mu}$. In Table 4 we summarize the numerical results of these cross section spectra.

To these spectra we fit a functional dependence $\sigma^{ee\to\Upsilon\to\mu\mu}(W_i,B_{\ell\ell},M_\Upsilon,w,\tilde{A})$, obtained from the DYMU2 generator for each c.m. energy W_i. The parameter set $(B_{\ell\ell},M_\Upsilon,w,\tilde{A})$ is sufficient to describe this process since, if we assume lepton universality $B_{\ell\ell}=B_{\mu\mu}=B_{ee}$, we can express all widths Γ, Γ_{ee}, and $\Gamma_{\mu\mu}$ in the nonradiative cross section σ_0 (Eq. (1)) in terms of $\tilde{A}$ and $B_{\ell\ell}$. We run the DYMU2 generator twice: first, with the full expression of σ_0, and second, removing the respective resonance amplitude in the event generation. By subtracting the latter cross section from the former, we obtain a fit function based on the third and second term in Eq. (1), which describe the resonance decays and their interference with the continuum, respectively. As already described above, the generator includes corrections for vacuum polarization and convolutions with the Gaussian distribution of the c.m. energy and with a Bremsstrahlung spectrum accounting for initial state photon radiation. The vacuum polarization correction to the nonradiative cross section is done such that all widths are physical quantities containing all contributions of higher order diagrams.

The fit function is completely insensitive to the total width $\Gamma = \tilde{A}/B_{\ell\ell}^2$ since $\Gamma \ll w$. Thus $B_{\ell\ell}$ enters only via the relative size $\alpha/3B_{\ell\ell}$ of the interference term compared to the resonance term (cf. the discussion after Eq. (1)). The fit result for $\tilde{A}$ depends only weakly on the size of the interference term, since our high-statistics data points are taken at c.m. energies where the net interference effect is small. We thus fix the ratio of resonance and interference term by setting $B_{\ell\ell}$ equal to its table values [13]. For M_Υ we also use the values from the Particle Data Group. The c.m. energy spread w has been fixed to the values from Table 1, which were obtained from fits to our hadronic cross section, as depicted in Figs. 2(a) and 3(a). These fits were performed without an interference contribution, since the maximum corrections to the observed hadronic cross section due to interference are only about 1% of the height of the resonance excitation curves.

We now fit the DYMU2 prediction to the measured $\sigma^{ee\to\Upsilon\to\mu\mu}(W)$ with $\tilde{A}$ as the only free parameter. From these fits shown as solid lines in Figs. 2(b) and 3(b), we obtain

$$\frac{\Gamma_{\mu\mu}\Gamma_{ee}}{\Gamma}(1S) = (31.2 \pm 1.6 \pm 1.7)\ \mathrm{eV}$$

and

$$\frac{\Gamma_{\mu\mu}\Gamma_{ee}}{\Gamma}(2S) = (6.5 \pm 1.5 \pm 1.0)\ \mathrm{eV}.$$

The systematic error sources for the calculation of $\tilde{A}$ are essentially the same as in our determination of $B_{\mu\mu}$. Only the statistical error on the number of multi-hadron events and the systematic error on the hadron selection efficiency do not enter. An uncertainty of 0.5 MeV in the c.m. energy of each data point was taken into account in the fit. In addition, the uncertainties in w contribute 2.3% and 3.4% to our systematic error on $\tilde{A}$ for the $\Upsilon(1S)$ and the $\Upsilon(2S)$, respectively. A 2.5% systematic error originates from the luminosity measurement. The error induced from fixing $B_{\ell\ell}$ is negligibly small. We find a change of only 1% for $\tilde{A}$ if we modify $B_{\ell\ell}$ by 40%. The errors on $B_{\ell\ell}$ from Ref. [13] therefore induce negligible errors of 0.1% for $\tilde{A}(1S)$ and 0.5% for $\tilde{A}(2S)$. Note that this also means that our determination of $\tilde{A}$ is essentially independent from the assumption of lepton universality in the utilization of Eq. (1). All $B_{\ell\ell}$ terms in this formula arise from setting $\sqrt{B_{ee}B_{\mu\mu}} \equiv B_{\ell\ell}$. Since $1.4B_{\ell\ell} = \sqrt{(2B_{ee})B_{\mu\mu}} = \sqrt{B_{ee}(2B_{\mu\mu})}$, a violation of lepton universality by a factor of 2 has the same 1% effect on $\tilde{A}$ as a change of 40% in $B_{\ell\ell}$.

By omitting the interference term in the generation of the μ-pair cross section, we can study whether this term is really necessary to describe our data. The corresponding fit results are shown as dashed lines in Figs. 2(b) and 3(b). On the $\Upsilon(2S)$ resonance we do not have sufficient statistics to discriminate between the hypotheses with and without interference. For the $\Upsilon(1S)$ we perform fits with and without interference under various assumptions concerning the correlation of errors. In all fits the hypothesis which includes interference is favoured by a likelihood ratio of at least 97:3. This is the first indication of the expected interference between muonic Υ decays and the continuum process $e^+e^- \to \mu^+\mu^-$. Following the arguments already made for the J/ψ [25], we thus confirm the assignment of $J^{PC} = 1^{--}$ for the $\Upsilon(1S)$.

The evidence for interference crucially depends on the size of $\Delta W = 0.5$ MeV, since an uncertainty of a few MeV would destroy its significance. We gain confidence in our determination of the energy scale by the facts that the fit to the hadronic cross section fixes the $\Upsilon(1S)$ mass with a precision of 0.2 MeV (see Table 1), and that this fit does not allow a shift of the two high-statistics data points at 9448.4 MeV and 9471.2 MeV by more than 0.5 MeV to lower values of W.

Discussion and Conclusions

Our determination of $B_{\mu\mu}(1S)$ and $B_{\mu\mu}(2S)$ is the first measurement that takes into account the interference between resonant and nonresonant μ-pair production. We obtain

$$B_{\mu\mu}(1S) = (2.31 \pm 0.16)\%$$

and

$$B_{\mu\mu}(2S) = (1.22 \pm 0.34)\%.$$

The only previous measurements that are clearly unaffected by interference are the $B_{\mu\mu}(1S)$ values of $(2.90 \pm 0.25 \pm 0.20)\%$ [32] and $(2.30 \pm 0.25 \pm 0.13)\%$ [34], determined using decays of the $\Upsilon(2S)$ to $\pi\pi\Upsilon(1S)$. Combining our values with all of the previous measurements listed in Table 5 leads to new world average values of $B_{\mu\mu}(1S) = (2.52 \pm 0.07)\%$ and $B_{\mu\mu}(2S) = (1.30 \pm 0.21)\%$, where statistical and systematic errors are added in quadrature.

We have determined for the first time from the energy dependence of the μ-pair cross section the product $\Gamma_{\mu\mu}\Gamma_{ee}/\Gamma$ for the $\Upsilon(1S)$ and the $\Upsilon(2S)$. Our results

$$\frac{\Gamma_{\mu\mu}\Gamma_{ee}}{\Gamma}(1S) = (31.2 \pm 2.3)\ \text{eV}$$

and

$$\frac{\Gamma_{\mu\mu}\Gamma_{ee}}{\Gamma}(2S) = (6.5 \pm 1.8)\ \text{eV}$$

are essentially independent of the assumption of lepton universality. They are in good agreement with the values (33.8 ± 1.4) eV and (7.6 ± 1.3) eV, derived from the world averages for Γ_{ee} [13] and $B_{\mu\mu}$ of the $\Upsilon(1S)$ and the $\Upsilon(2S)$, respectively.

The fits to the energy dependence of the cross section for resonant μ-pair production in the $\Upsilon(1S)$ region favour interference with the continuum by a likelihood ratio of at least 97:3. This is the first indication of such an interference in the Υ system, as expected for the $J^{PC} = 1^{--}$ assignment for the $\Upsilon(1S)$.

Our measurements of $B_{\mu\mu}$ and $\Gamma_{\mu\mu}\Gamma_{ee}/\Gamma$ can be used, together with other published values, to obtain individual widths of the Υ resonances. Some care must be taken about the independence of the quantities involved in these calculations. For example, our results should not be used to calculate the electronic widths of the Υ resonances according to $\Gamma_{ee} = (\Gamma_{\mu\mu}\Gamma_{ee}/\Gamma)/B_{\mu\mu}$, since the errors of the two measurements are strongly correlated. Rather, Γ_{ee} has to be determined directly from the hadronic cross section, which we have already done in Ref. [15]. We show now how our results can be used to obtain $\Gamma_{\mu\mu}(1S)$, $\Gamma(1S)$, and $\Gamma(2S)$.

We divide our result on $\Gamma_{\mu\mu}\Gamma_{ee}/\Gamma(1S)$ by the world average value of $B_{ee}(1S) = (2.52 \pm 0.17)$ %, which has been obtained independently of $B_{\mu\mu}$ measurements [13]. Thereby we

obtain for the first time independent of Γ_{ee} and $B_{\mu\mu}$ measurements the muonic width

$$\Gamma_{\mu\mu}(1S) = (1.24 \pm 0.06 \pm 0.11) \text{ keV}.$$

The systematic error on $\Gamma_{\mu\mu}(1S)$ is dominated by the error on B_{ee}. This result is in good agreement with the value $\Gamma_{\mu\mu}(1S) = \Gamma_{ee}(1S)B_{\mu\mu}(1S)/B_{ee}(1S) = (1.34 \pm 0.11)$ keV, which is derived from the current world average values. By comparing our measurement with the world average value [13] of $\Gamma_{ee}(1S) = (1.34 \pm 0.04)$ keV, we test lepton universality, because our value for $\Gamma_{\mu\mu}(1S)$ relies on lepton universality just as little as our measurement of $\Gamma_{\mu\mu}\Gamma_{ee}/\Gamma(1S)$.

Assuming lepton universality, we can combine both values to $\Gamma_{\ell\ell}(1S) = (1.33 \pm 0.04)$ keV. Together with the new world average over all three leptonic branching ratios $B_{\ell\ell}(1S) = (2.53 \pm 0.06)$ %, we find the total width $\Gamma(1S) = \Gamma_{\ell\ell}(1S)/B_{\ell\ell}(1S) = (52.5 \pm 1.9)$ keV.

For the $\Upsilon(2S)$ resonance we cannot derive $\Gamma_{\mu\mu}(2S)$ from our analysis, since $B_{ee}(2S)$ has not yet been measured. (The value listed in [13] has been derived from $B_{ee}=\Gamma_{ee}/\Gamma$, and Γ has been calculated from $\Gamma_{ee}/B_{\ell\ell}$, where $B_{\ell\ell}$ is strongly dominated by the value of $B_{\mu\mu}$. Thus B_{ee} and $B_{\mu\mu}$ are not independent measurements [26].) We use the new average of $B_{\mu\mu}(2S)$ to recalculate $\Gamma_{ee}(2S) = (0.584 \pm 0.028)$ keV after Ref. [13] and determine the total width $\Gamma(2S) = \Gamma_{ee}(2S)/B_{\mu\mu}(2S) = (45.0 \pm 7.5)$ keV, where again lepton universality is assumed.

Acknowledgements

We thank J.E. Campagne for explaining details of the DYMU2 generator to us. We would like to thank the DESY and SLAC directorates for their support. This experiment would not have been possible without the dedication of the DORIS machine group as well as the experimental support groups at DESY. The visiting groups thank the DESY laboratory for the hospitality extended to them. Z.J., T.L., B.Muryn, B.N., and G.N. thank DESY for financial support. E.D.B., R.H., and K.S. have benefitted from financial support from the Humboldt Foundation. K. Königsmann acknowledges support from the Heisenberg Foundation.

References

[1] P.B. Mackenzie and G.P. Lepage, Phys. Rev. Lett. 47 (1981) 1244.
W. Kwong, P.B. Mackenzie, R. Rosenfeld, and J.L. Rosner, Phys. Rev. D37 (1988) 3210.

[2] S.J. Brodsky, P.B. Mackenzie, and G.P. Lepage, Phys. Rev. D28 (1983) 228.
D.W. Duke and R.G. Roberts, Phys. Reports 120 (1985) 277.

[3] E.D. Bloom and C.W. Peck, Ann. Rev. Nucl. Part. Sci. 33 (1983) 143.

[4] K. Wachs et al., Z. Phys. C42 (1989) 33.

[5] Z. Jakubowski and M. Kobel, Nucl. Instr. Meth. A297 (1990) 60.

[6] J.E. Campagne and R. Zitoun, Z. Phys. C43 (1989) 469.

[7] In J.E. Campagne and R. Zitoun, Paris preprint, LPNHEP-88.06 (1988),
and J.E. Campagne, Ph.D. Thesis, Universites de Paris VI et VII (1989)
the authors have modified the structure function approach of
E.A. Kuraev and V.S. Fadin, Sov. J. Nucl. Phys. 41 (1985) 466
in order to reproduce the exact second order results of
F.A. Berends, G.J.H. Burgers, and W.L. van Neerven, Nucl. Phys. B297 (1988) 429
and erratum Nucl. Phys. B304 (1988) 921.

[8] M.Kobel, Ph.D. Thesis, Universität Erlangen-Nürnberg, (1991),
DESY internal report F31-91-03.

[9] F.A. Berends and G.J. Komen, Phys. Lett. 63 B (1976) 432,
based on the subroutine PIHINT from the MMG1 generator [24].

[10] F.A. Berends and G.J. Komen, Nucl. Phys. B115 (1976) 114.

[11] H. Fesefeldt, Aachen preprint, PITHA-85/02 (1985).

[12] R. Ford and W. Nelson, SLAC-210 (1978).

[13] Particle Data Group: Review of Particle Properties, Phys. Lett. B 239 (1990) 1.

[14] D.P. Barber et al., Phys. Lett. B 135 (1984) 498.

[15] Z. Jakubowski et al., Z. Phys. C40 (1988) 49.

[16] F.A. Berends and R. Kleiss, Nucl. Phys. B228 (1983) 537
and Nucl. Phys. B186 (1981) 22.

[17] K.Wachs, Ph.D. Thesis, Universität Hamburg, (1988), DESY internal report F31-88-01.

[18] F.A. Berends, P.H. Daverfeldt, and R. Kleiss, Comp. Phys. Comm. 40 (1986) 271.

[19] J.A.M. Vermaseren, Nucl. Phys. B229 (1983) 347.

[20] S.J. Brodsky, T. Kinoshita, and H. Terazawa, Phys. Rev. D4 (1971) 1532.

[21] S. Jadach and Z. Wąs, Comp. Phys. Comm. 36 (1985) 191.

[22] S. Lowe, Ph.D. Thesis, Stanford University (1986).

[23] T. Sjöstrand, Comp. Phys. Comm. 39 (1986) 347,
T. Sjöstrand and M. Bengtsson, Comp. Phys. Comm. 43 (1987) 367.
We compare the colour string fragmentation of the JETSET 6.2 version with the JETSET 6.3 program modeling parton shower fragmentation.

[24] R. Kleiss, Ph.D. Thesis, Rijksuniversiteit te Leiden (1982);
F.A. Berends, R. Kleiss, and S. Jadach, Nucl. Phys. B202 (1982) 63.

[25] A.M. Boyarski et al., Phys. Rev. Lett. 34 (1975) 1357.

[26] K.R. Schubert, private communication.

[27] Ch. Berger et al., Z. Phys. C1 (1979) 343.

[28] P. Bock et al., Z. Phys. C6 (1980) 125

[29] B. Niczyporuk et al., Z. Phys. C15 (1982) 299.

[30] H. Albrecht et al., Phys. Lett. 116 B (1982) 383.

[31] D. Andrews et al., Phys. Rev. Lett. 50 (1983) 807.

[32] D. Besson et al., Phys. Rev. D30 (1984) 1433.

[33] T. Kaarsberg et al., Contr. Paper #286 to Int. Symp. on Lepton and Photon Interactions, Hamburg (1987).

[34] H. Albrecht et al., Z. Phys. C35 (1987) 283.

[35] T. Kaarsberg et al., Phys. Rev. Lett. 62 (1989) 2077.

[36] W.-Y. Chen et al., Phys. Rev. D39 (1989) 3528.

[37] P. Haas et al., Phys. Rev. D30 (1984) 1996.

[38] H. Albrecht et al., Z. Phys. C28 (1985) 45.

Table Captions

1. Resulting parameters from the fit to the observed hadronic cross section in Figs. 2(a) and 3(a).

2. Summary of results for the calculation of $B_{\mu\mu}$.

3. Fractional influences of the various error sources on the errors of our $B_{\mu\mu}$ measurements.

4. The efficiency corrected cross section for $e^+e^- \to \Upsilon(1S) \to \mu^+\mu^-$ and $e^+e^- \to \Upsilon(2S) \to \mu^+\mu^-$ at the DORIS II storage ring as a function of the c.m. energy W, as displayed in Figs. 2(b) and 3(b). We list only those errors on the cross section which are essentially independent from point to point. Statistical and systematic errors have been added in quadrature. The latter include the error on W, converted to an error on the cross section. Additional errors common to all points are fractional errors of 3.6% for the $\Upsilon(1S)$ data and 4.2% for the $\Upsilon(2S)$ data, and absolute errors of 6.4 pb and 5.6 pb, respectively. These additional errors are at least a factor of three smaller than the smallest point-to-point uncertainties.

5. Summary of $B_{\mu\mu}$ measurements. We disentangled the CLEO value of $B_{\ell\ell}(1S) = (2.84 \pm 0.18 \pm 0.20)$ % from [32] into a value for $B_{ee}(1S) = (2.77 \pm 0.25 \pm 0.20)$ % and the listed value for $B_{\mu\mu}(1S)$. The ARGUS $\Upsilon(2S)$ value is scaled from the average $\Upsilon(1S)$ value with $B_{\mu\mu}(2S) = 1.57 \pm 0.59 \pm 0.53 + 2.1(B_{\mu\mu}(1S)-2.9)$ (in %) [38].

Figure Captions

1. a) Observed cross section for μ pairs and b) the prediction of the continuum background versus c.m. energy W. The background prediction is the sum of all continuum background processes. It does not include resonant processes $\Upsilon \to \mu\mu$+X. The fluctuations arise from variations of the detector acceptance with time. The dotted curves show expectations for a constant detector acceptance. A good correlation between the data (a) and the background prediction (b) is observed from the respective variation of the high statistics points around these dotted lines.

2. a) Observed hadronic cross section in the region of the $\Upsilon(1S)$ resonance. The solid line is a fit giving the parameters listed in Table 1. The dotted line shows the continuum contribution $\sigma^{ee\to qq}$ to the fit. b) Measured cross section of $e^+e^- \to \Upsilon \to \mu^+\mu^-$ in the region of the $\Upsilon(1S)$ resonance. It has been obtained by subtracting from the observed μ-pair cross section of Fig. 1(a) the continuum background prediction of Fig. 1(b),

scaled with $C = 0.999$, plus a small resonant background. The resulting spectrum was corrected point-by-point with the detection efficiency $\epsilon_i^{\Upsilon \to \mu\mu}$. We only show those errors which are independent point to point (see Table 4). The lines are fitted to the cross section as described in the text. The dashed line is a fit without interference; the solid line is a fit with interference.

3. Same as Figure 2, but for the region of the $\Upsilon(2S)$ resonance.

Table 1:

		Υ(1S)	Υ(2S)
M_Υ	(MeV/c^2)	9460.3 $\pm$ 0.2	10023.2 $\pm$ 0.3
w	(MeV)	7.9 $\pm$ 0.2	8.2 $\pm$ 0.3
$\sigma^{\Upsilon\to had}(W_{peak})$	(pb)	9566 $\pm$ 58	3263 $\pm$ 51
$\sigma^{ee\to qq}(W_{peak})$	(pb)	3544 $\pm$ 22	3267 $\pm$ 47

Table 2:

	Υ(1S)	Υ(2S)
$\sum N_i^{\mu\mu}$	18680 $\pm$ 140	16076 $\pm$ 130
$- C\sum \mathcal{L}_i\sigma_i^{BG}$	15477 $\pm$ 82 $\pm$ 104	15404 $\pm$ 82 $\pm$ 101
$- \sum N_i^{\Upsilon\to\mu\mu X}$	14 $\pm$ 0 $\pm$ 2	15 $\pm$ 0 $\pm$ 9
$\sum N_i^{\Upsilon\to\mu\mu}$	3189 $\pm$ 162 $\pm$ 104	657 $\pm$ 154 $\pm$ 101
$\sum N_i^{\Upsilon\to\mu\mu}/\varepsilon_i^{\Upsilon\to\mu\mu}$	7143 $\pm$ 364 $\pm$ 295	1491 $\pm$ 350 $\pm$ 232
$- \sum \mathcal{L}_i\sigma_i^I$	$-80 \pm 0 \pm 72$	$-29 \pm 0 \pm 30$
$\mathcal{N}(\Upsilon\to\mu\mu)$	7223 $\pm$ 364 $\pm$ 304	1520 $\pm$ 350 $\pm$ 234
: $\mathcal{N}(\Upsilon)$ / 10^3	313.2 $\pm$ 1.1 $\pm$ 4.4	125.0 $\pm$ 1.9 $\pm$ 2.1
$B_{\mu\mu}$ / %	2.31 $\pm$0.12 $\pm$0.10	1.22 $\pm$0.28 $\pm$0.19

Table 3:

statistical errors	Υ(1S)	Υ(2S)
$\Delta N^{\Upsilon\to had}$	0.4%	1.6%
$\Delta N_{off}^{\mu\mu}$	2.5%	12.3%
$\Delta N_i^{\mu\mu}$	4.3%	19.5%
total $\Delta B_{\mu\mu}/B_{\mu\mu}$	5.0%	23.1%
systematic errors	**Υ(1S)**	**Υ(2S)**
$\Delta N^{\Upsilon\to\mu\mu X}$	0.1%	1.3%
$\Delta\varepsilon^{\Upsilon\to all}$	1.4%	1.7%
ΔW	1.0%	1.9%
$\Delta\varepsilon^{\Upsilon\to\mu\mu}$	2.5%	2.5%
$\Delta(\mathcal{L}_i/\mathcal{L}_{off})$	1.2%	4.1%
$\Delta(\sigma_i^{BG}/\sigma_{off}^{BG})$	3.0%	14.5%
total $\Delta B_{\mu\mu}/B_{\mu\mu}$	4.4%	15.5%

Table 4:

$\Upsilon(1S)$				$\Upsilon(2S)$			
W (MeV)	ΔW (MeV)	$\sigma^{ee\to\Upsilon\to\mu\mu}$ (pb)	$\Delta\sigma^{ee\to\Upsilon\to\mu\mu}$ (pb)	W (MeV)	ΔW (MeV)	$\sigma^{ee\to\Upsilon\to\mu\mu}$ (pb)	$\Delta\sigma^{ee\to\Upsilon\to\mu\mu}$ (pb)
9362.9	2.0	19.5	19.7	9966.2	1.0	36.7	39.0
9388.3	0.5	186.4	175.5	9985.4	1.0	−70.9	142.3
9396.3	0.5	−148.5	145.7	10009.4	0.5	108.6	88.6
9407.4	0.5	−50.8	161.5	10014.6	0.5	−113.5	92.7
9416.9	0.5	−328.5	157.9	10018.4	0.5	111.1	106.5
9426.1	0.5	−208.5	161.0	10022.1	0.5	29.1	76.7
9436.2	0.5	-3.5	125.1	10023.3	0.5	18.0	18.8
9444.3	0.5	14.7	109.4	10023.9	0.5	45.3	17.0
9448.4	0.5	22.4	28.5	10024.6	1.0	63.7	17.3
9452.5	0.5	57.0	87.3	10028.2	0.5	67.6	32.6
9455.4	0.5	100.2	81.2	10029.5	0.5	−4.9	47.9
9457.5	0.5	198.7	36.5	10033.2	0.5	29.9	52.2
9459.1	0.5	218.1	31.5	10039.1	0.5	−30.7	110.3
9459.5	0.5	274.3	31.9				
9460.1	0.5	256.6	25.0				
9460.4	0.5	231.3	30.3				
9460.6	0.5	240.5	29.0				
9461.3	0.5	172.9	55.7				
9467.5	0.5	271.8	93.6				
9471.2	0.5	185.8	28.9				
9473.6	0.5	176.4	99.0				
9478.0	0.5	76.5	111.0				
9481.8	0.5	197.4	145.7				
9486.1	0.5	37.1	215.4				
9490.0	0.5	70.0	183.5				
9493.6	0.5	85.5	217.9				
9497.6	0.5	104.6	195.0				
9506.6	0.5	171.1	243.1				

Table 5:

Ref. Exp. Year	$B_{\mu\mu}$(1S) in %					Ref. Exp. Year	$B_{\mu\mu}$(2S) in %				
[27] PLUTO 79	2.2	$\pm$	2.0			[37] CLEO 84	1.8	$\pm$	0.8	$\pm$	0.5
[28] DESY-HD 80	1.4	$^{+}_{-}$	$^{3.4}_{1.4}$			[38] ARGUS 85	0.77	$\pm$	0.59	$\pm$	0.55
[29] LENA 82	3.8	$\pm$	1.5	$\pm$	0.2	[35] CUSB 89	1.38	$\pm$	0.25	$\pm$	0.15
[30] DASP 82	3.2	$\pm$	1.3	$\pm$	0.3						
[31] CLEO 83	2.7	$\pm$	0.3	$\pm$	0.3	Prev. Average	1.35	$\pm$	0.26		
[32] CLEO 84	2.90	$\pm$	0.25	$\pm$	0.20	This Experiment	1.22	$\pm$	0.28	$\pm$	0.19
[33] CUSB 87	2.70	$\pm$	0.28	$\pm$	0.14	New Average	1.30	$\pm$	0.21		
[34] ARGUS 87	2.30	$\pm$	0.25	$\pm$	0.13						
[35] CUSB 89	2.61	$\pm$	0.09	$\pm$	0.11						
[36] CLEO 89	2.52	$\pm$	0.07	$\pm$	0.07						
Prev. Average	2.57	$\pm$	0.07								
This Experiment	2.31	$\pm$	0.12	$\pm$	0.10						
New Average	2.52	$\pm$	0.07								

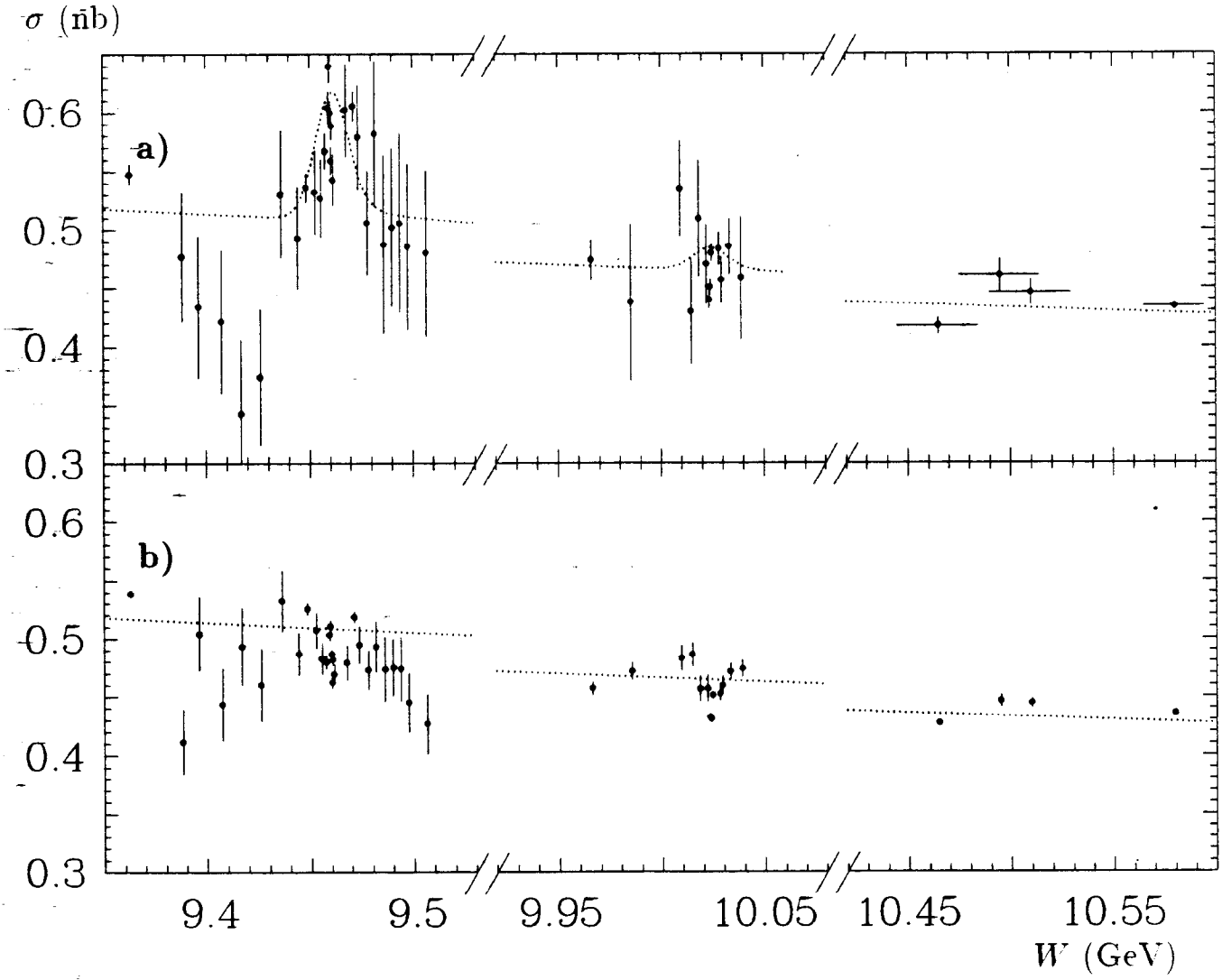

Figure 1

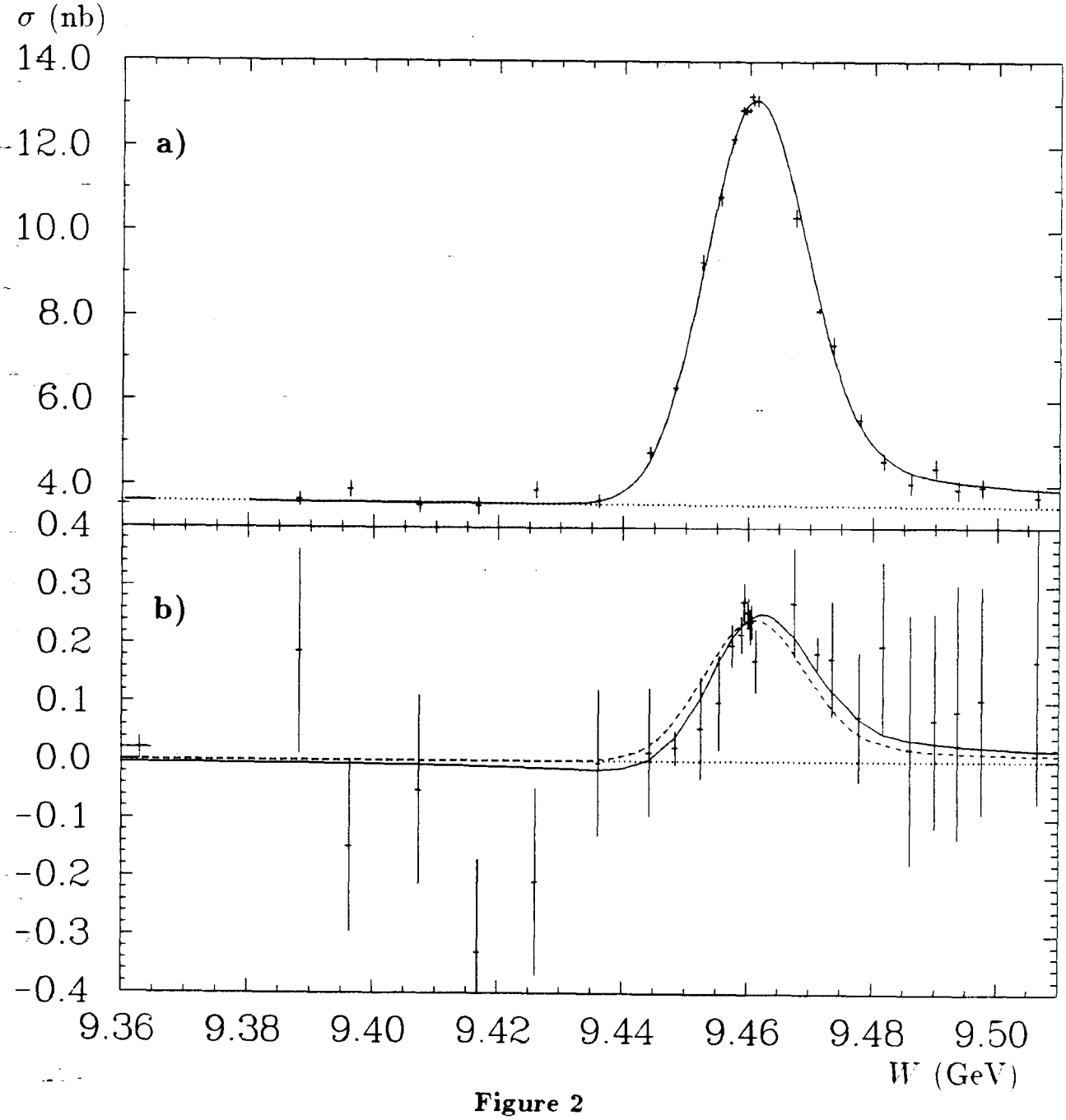
σ (nb)
14.0
12.0
10.0
8.0
6.0
4.0
a)
0.4
0.3
0.2
0.1
0.0
-0.1
-0.2
-0.3
-0.4
b)
9.36
9.38
9.40
9.42
9.44
9.46
9.48
9.50
W (GeV)

Figure 2

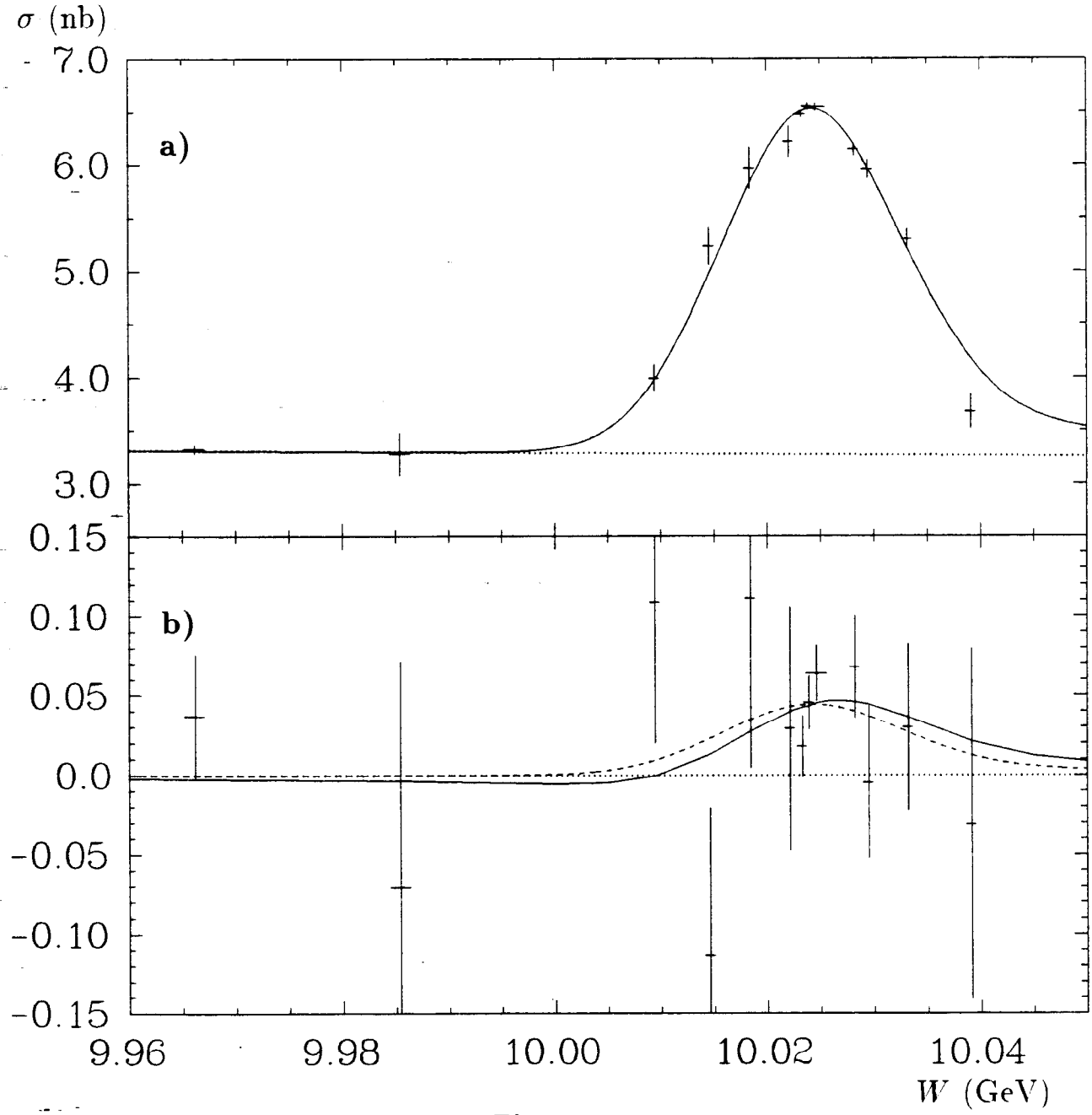
σ (nb)
7.0
6.0
5.0
4.0
3.0
a)
0.15
0.10
0.05
0.0
-0.05
-0.10
-0.15
b)
9.96
9.98
10.00
10.02
10.04
W (GeV)

Figure 3